1   Revision 1   2 May 2013

2

3   **Infrared signatures of OH-defects in wadsleyite: a first-principles study**

4

5   Marc Blanchard[1,*], Mathilde Roberge[1], Etienne Balan[1], Guillaume Fiquet[1]

6   and Hélène Bureau[1]

7

8   [1] Institut de Minéralogie et de Physique des Milieux Condensés (IMPMC), Université

9   Pierre et Marie Curie (Paris VI), CNRS UMR 7590, IRD UMR 206, Case 115, 4 place

10   Jussieu, 75252 Paris Cedex 05, France

11   *Communicating Author: Marc Blanchard. E-mail: marc.blanchard@impmc.upmc.fr

12

13

14   **Abstract**

15   The structure and the polarized infrared absorption spectrum of OH-defects in

16   wadsleyite (β-Mg$_2$SiO$_4$) are studied, at 0 and 15 GPa, by first-principles calculations

17   based on density functional theory (DFT). Four types of OH-defects are considered: fully

18   protonated magnesium vacancies, fully protonated silicon vacancies, silicon vacancies

19   compensated by a magnesium cation and two protons, and OH-defects associated with

20   the migration of a silicon cation to a normally vacant site, as reported by Kudoh and

21   Inoue (1999). The results suggest that the main absorption band constituted by a doublet

22   (3326 and 3360 cm^{-1}) corresponds to at least two types of OH-defects involving M3

23   vacancies with protonation of the O1-type oxygens along the O1...O4 edges. The main

1

24   contribution of the less intense band at 3581 cm^{-1} is likely related to the partial

25   protonation of a silicon vacancy (protonation of the O3-type oxygen) associated with the

26   migration of the silicon cation to the Si2 site. This assignment is consistent with several

27   experimental constraints: wavenumber and pleochroism of infrared OH-stretching bands,

28   pressure-dependence of the bands wavenumber, evidence from X-ray diffraction of

29   magnesium vacancies in M3 site, and increase of the *b*/*a* axial ratio with water content.

30   The integrated absorption coefficients of the corresponding OH-defects are also

31   calculated and thus complement the set of data obtained previously for forsterite and

32   ringwoodite. Absorption coefficients of wadsleyite computed at 0 and 15 GPa indicate

33   that for a precise quantification of the hydrogen content in *in situ* experiments, one must

34   consider higher absorption coefficients than those determined at 0 GPa after quench. It is

35   also shown that a single theoretical relation can account for the three Mg$_2$SiO$_4$

36   polymorphs at 0 GPa: K$_{int}$ = 278.7±18.1 (3810±465 - x), where K$_{int}$ is the integrated

37   molar absorption coefficient of the OH stretching modes and x is the average

38   wavenumber in cm^{-1}. Absorption coefficients are significantly lower than the general

39   calibrations, the use of which would lead to an underestimation of the water

40   concentrations.

41

42   **Keywords:** wadsleyite, OH-defect, IR spectroscopy, *ab initio* calculations, DFT

43

1. INTRODUCTION

The interest for OH-defects in nominally anhydrous minerals (NAMs) is essentially two-fold. First, given the abundance of the NAMs in the mantle, these OH-defects may contribute significantly to the water budget of the Earth. Second, the presence of OH-defects within the structure of NAMs modifies the bulk properties of minerals. These hydroxyl groups may affect the global mantle dynamics because hydrogen incorporation is likely to change melting temperatures, atomic diffusivities, and rheological properties. In addition, it is essential to know the effect of OH-defects on electrical conductivity and elasticity of minerals for interpreting accurately the geophysical properties that are used to probe the Earth interior (Keppler and Smyth, 2006).

Wadsleyite corresponds to a high-pressure polymorph of forsterite. It is considered to be the dominant mineral in the upper part of the transition zone between 410 and 520 km depth, before its transformation into ringwoodite at higher pressure. The structure of hydrogen-free wadsleyite (β-Mg_2SiO_4) can be refined in the orthorhombic *Imma* space group, with the following cell parameters: a = 5.698 Å, b = 11.438 Å, and c = 8.257 Å (Horiuchi and Sawamoto, 1981). Silicon atoms in tetrahedral sites (Wyckoff position *8h*) form Si_2O_7 groups (sorosilicate). There are three distinct octahedral sites occupied by magnesium atoms, M1 (*4a*), M2 (*4e*), and M3 (*8g*), with twice as many M3 sites as M1 or M2 sites in each unit cell. M1 and M2 sites share edges and form a single octahedral chain, which runs parallel to the *b*-axis. M3 octahedra form a double chain running along the *a*-axis. Finally, there are four distinct oxygen sites in the structure.

67   Among them, O2 is the bridging oxygen of the Si_2O_7 group, and O1 is a non-silicate

68   oxygen atom (not bonded to silicon atoms). This structural feature makes the O1 atoms

69   strongly underbonded with a valence of 1.82 valence units (v.u.) using the method of

70   Donnay and Allmann (1970), and for this reason O1 atoms are expected to be very

71   favourable sites for protonation (Smyth, 1987). The ability of wadsleyite to incorporate

72   significant amount of hydrogen has been confirmed experimentally (e.g. McMillan et al.

73   1991, Young et al. 1993, Inoue et al. 1995, Kohlstedt et al. 1996, Kohn et al. 2002,

74   Demouchy et al. 2005, Ye et al. 2010). A review of the water content in wadsleyite

75   quantified by secondary ion mass spectrometry can be found in Demouchy et al. (2005),

76   and highlights the variability of water contents obtained experimentally. Demouchy et al.

77   (2005) have shown that the water solubility in Fe-free wadsleyite decreases with

78   increasing temperature, from ~2.2 wt % H_2O at 900°C down to ~0.9 wt % H_2O at 1400°C

79   (15 GPa). On the other hand, no significant effect of pressure was observed.

80   The knowledge of the location of hydrogen within the crystal structure is a

81   prerequisite to understand the mechanisms controlling the changes of mineral bulk

82   properties. Because of the low hydrogen concentrations, it is not possible to determine

83   experimentally the protons location using for instance diffraction techniques. In this field,

84   modeling techniques proved to be very useful. Several theoretical studies have

85   investigated the mechanisms of hydrogen incorporation via the formation of OH-defects

86   within the wadsleyite structure (Winkler et al. 1995, Wright and Catlow 1996, Haiber et

87   al. 1997, Ross et al. 2003, Parker et al. 2004, Walker et al. 2006, Tsuchiya and Tsuchiya

88   2009, Verma and Karki 2009). Based on total energy calculations and on vibrational

89   frequencies, the proposed models imply the protonation of magnesium and silicon

90   vacancies. In the present work, we propose to test different models of OH-defects with

91   the calculation of the relative intensities and the polarization of the infrared (IR)

92   absorption bands of OH-stretching modes at 0 and 15 GPa. This approach will enable a

93   direct comparison with experiment, and so the interpretation of the major IR absorption

94   bands of wadsleyite, which can be considered as the most discriminating signatures of

95   OH-defects in this mineral.

96

97   **2. THEORETICAL METHODS**

98

99   Calculations are done on a 2×1×1 supercell of wadsleyite (i.e. 112 atoms)

100   containing up to four hydrogen atoms. This corresponds to a maximum hydrogen

101   concentration of 1.65 wt % H_2O. With ~10 Å between the neutral OH-defect and its

102   periodic images in the three directions, the OH-defect can be considered as sufficiently

103   isolated to account for experimental samples displaying lower hydrogen concentrations.

104   Calculations are performed within the density functional theory framework, using the

105   generalized gradient approximation (GGA) to the exchange-correlation functional with

106   the PBE parametrization (Perdew et al. 1996) and periodic boundary conditions. The

107   ionic cores are described by the ultrasoft pseudopotentials Si.pbe-rrkjus.UPF, O.pbe-

108   rrkjus.UPF, and H.pbe-rrkjus.UPF from http://www.quantum-espresso.org and the

109   magnesium norm-conserving pseudopotential previously used to model forsterite,

110   ringwoodite and enstatite (Blanchard et al. 2009, Balan et al. 2011, 2012). The electronic

111   wave-functions and the charge density are expanded in plane-waves with 60 and 600 Ry

112   cutoffs, respectively. For the electronic integration, the Brillouin zone is sampled using a

5

113     $2 \times 2 \times 2$ k-point grid according to the Monkhorst-Pack scheme (Monkhorst and Pack

114   1976). It is checked that increasing the wave-functions cutoff to 100 Ry and using a 4×4

115     $\times 4$ k-point grid does not change the total energy by more than 1.1 meV/atom and does

116   not modify significantly the residual forces on atoms. Atomic relaxations are performed

117   with the PWscf code (Giannozzi et al., 2009; http://www.quantum-espresso.org) until the

118   residual forces on atoms are less than 10^{-4} Ry/a.u.. The optimized cell parameters are

119   only slightly smaller than the experimental ones, i.e. $a = 5.691$ Å, $b = 11.428$ Å, and $c =$

120   8.240 Å (this work) versus $a = 5.698$ Å, $b = 11.438$ Å, and $c = 8.257$ Å (Horiuchi and

121   Sawamoto, 1981). Defective structures are fully relaxed at constant pressure (at 0 and 15

122   GPa), by optimizing the atomic positions as well as the cell parameters. This approach

123   allows assessing the evolution of the cell parameters associated with the protonation

124   mechanisms.

125   The dynamical matrix and dielectric quantities, such as the Born effective charges

126   and the electronic dielectric tensor, are calculated at the Brillouin zone center (Γ point),

127   within the harmonic approximation using the linear response theory (Baroni et al. 2001)

128   as implemented in the PHonon code (Giannozzi et al., 2009; http://www.quantum-

129   espresso.org). The high-frequency OH-stretching modes can be accurately calculated by

130   only considering the displacement of the oxygen and hydrogen atoms involved in OH

131   groups (Balan et al. 2005). We note that the anharmonicity of OH modes is not explicitly

132   considered here. However, a reasonable agreement with experimental frequencies (i.e.,

133   within ~ 1 rel.%) can be expected due to the cancelation of the error related to the neglect

134   of anharmonicity with that related to the use of the GGA approximation (Balan et al.

135   2007; Finocchi et al. 2008). The complex low-frequency dielectric permittivity tensor is

6

136   calculated for each defect by including only the contributions of OH-stretching modes

137   and electronic polarizability, using an arbitrary damping parameter of 2 cm^{-1}. The

138   polarized IR absorption spectra along the *a*, *b*, and *c*-axis were then calculated using the

139   corresponding diagonal elements of the low-frequency dielectric tensor. The integrated

140   molar absorption coefficients are also computed for the OH-defects.

141

142   **3. EXPERIMENTAL CONSTRAINTS ON OH-DEFECTS IN WADSLEYITE**

143

144   Diffraction techniques and vibrational spectroscopies are not able to determine

145   unambiguously the atomic configuration of OH-defects, but they provide crucial

146   constraints on the nature of OH-defects. For wadsleyite, the proposed atomic models will

147   have to take into account or reproduce the four following experimental constraints:

148   (i) IR spectroscopy is the most widely used technique to investigate the concentration and

149   the nature of OH-defects in minerals. Several IR spectra, most of the time unpolarized, of

150   protonated wadsleyite are reported in the literature (e.g. Young et al. 1993, Kohlstedt et

151   al. 1996, Bolfan-Casanova et al. 2000, Kohn et al. 2002, Jacobsen et al. 2005, Deon et al.

152   2010). We will refer here to the polarized IR spectra measured by Jacobsen et al. (2005)

153   on wadsleyite samples containing between ~100 and ~10000 wt ppm H_2O (Fig. 1). In the

154   absorption range of OH-stretching modes, we can distinguish two main groups of bands;

155   the more intense group being the one at lower wavenumber. Each group is composed by

156   at least two absorption bands. The first group displays two bands at 3326 and 3360 cm^{-1}

157   (here referred to as bands A and B, respectively) that both show a minimal pleochroism

158   even if the maximum intensities occur for a polarization along the *c*-axis. The second

159   group has a band at 3581 cm^{-1} (referred to as band C) that is polarized in the *bc* plane and

160   another band at 3614 cm^{-1} of smaller intensity (referred to as band D), polarized in the *ac*

161   plane. It is important to note that at very low concentration (~150 wt ppm H$_2$O) the OH

162   spectrum is relatively simple. Only one absorption band is present in each region, i.e. the

163   band D and the band A, which is in fact a doublet with a contribution at 3317 cm^{-1}

164   polarized along the *b*-axis and a contribution at 3324 cm^{-1} polarized in the *ac* plane. In

165   addition to these main bands, we can note a broad absorption band centered around 3000

166   cm^{-1} with a maximum intensity for the polarization along the *a*-axis, as well as small

167   features between the two main groups of bands and shoulders to these main bands. Some

168   studies have also reported extra bands at high wavenumbers, ~3660 cm^{-1}, but their

169   intensities are relatively weak (Bolfan-Casanova et al. 2000, Kohn et al. 2002, Deon et al.

170   2010). The observation of IR spectra thus suggests the presence of several types of OH-

171   defects with a more diverse population when hydrogen content increases.

172   (ii) Deon et al. (2010) measured the IR spectrum of a synthetic wadsleyite containing

173   ~8000 wt ppm H$_2$O, from ambient conditions up to 15.4 GPa. Essentially, the low-

174   wavenumber group of bands shifts strongly toward lower wavenumbers (~ -8 cm^{-1}/GPa),

175   whereas the position of the high-wavenumber group of bands remains about constant (~

176   +0.3 cm^{-1}/GPa). In their Raman spectroscopic study, Kleppe et al. (2001) found very

177   similar pressure dependences for a sample containing 1.65 wt % H$_2$O.

178   (iii) Structure refinements from single-crystal X-ray diffraction measurements show that

179   most of the cation vacancies are located on the M3 sites (Kudoh and Inoue 1999, Deon et

180   al. 2010, Ye et al. 2010), and that this amount of M3 vacancies increases with increasing

181   water content (Jacobsen et al. 2005). This is consistent with theoretical results, which

8

182   suggest that the most favorable OH-defect is the doubly-protonated M3 vacancy while in

183   the anhydrous system, M1 is the most favorable site for the formation of Mg vacancy

184   (Walker et al. 2006). Kudoh and Inoue (1999) also find some experimental indications of

185   vacancies at M2 sites. In addition and in agreement with Smyth et al. (1997), they report

186   a partial occupancy by silicon of a normally vacant tetrahedral site (Si2) adjacent to M3

187   site. Smyth et al. (1997) assume that this is the result of a six-fold silicon moving from

188   M3 site to the adjacent tetrahedral void on decompression whereas Kudoh and Inoue

189   (1999) consider that the silicon atom has migrated from the Si site in association with the

190   vacancy at M3 site.

191   (iv) Jacobsen et al. (2005) also investigated the evolution of the cell parameters as a

192   function of water content. Whereas the a and c dimensions decrease slightly with

193   increasing water content, the b dimension increases much significantly, providing the

194   following empirical relation:

195    $(b/a) = 2.008(1) + 1.25(3) \times 10^{-6} \cdot C_{H_2O}$

196   where C_{H_2O} is the concentration of water in ppm H_2O by weight.

197

198   **4. RESULTS**

199

200   **4.1. Protonated magnesium vacancies**

201   We focus here on both M2 and M3 vacancies. In total, about twenty starting

202   defect configurations are investigated. In agreement with previous theoretical data (e.g.

203   Walker et al. 2006), the most stable defect, i.e. $V_{M3}\_O1\_O1$, corresponds to a M3

204   vacancy with protonation of O1-type oxygens, which are the non-silicate oxygens already

9

205   strongly underbonded in the non-defective structure. The two OH bonds point toward the

206   apical O4 atoms of this vacancy and have similar bond lengths (Fig. 2, Table 1). This

207   leads to a coupling of OH motions with an in-phase stretching mode at 3367 cm^{-1} that is

208   polarized along the *b*-axis and an out-of-phase stretching mode at 3374 cm^{-1}, mainly

209   polarized in the *ac* plane. Overall this doublet displays its strongest contribution along the

210   *c*-axis.

211   The second most stable configuration for a protonated magnesium vacancy still

212   involves a M3 site and corresponds to V_{M3}_O1_O3. It differs from the previous OH-

213   defect by one of the two protons that is now located between the two O3 oxygens and is

214   0.37 eV less stable. This energy difference implies that, even at high temperatures

215   relevant to the mantle transition zone, the probability of occurrence of this configuration

216   is small (less than 10 %). Bond valence analysis using the method of Donnay and

217   Allmann (1970) evidences that the creation of a M3 vacancy leaves O1 and O3 oxygens

218   with residual valence of 1.46 and 1.67 v.u., respectively. The loosely bound proton (O3-

219   H = 1.022 Å) gives rise to an absorption band at 2837 cm^{-1} polarized along the *a*-axis. In

220   this OH-defect, the small relaxation of the O1-H…O4 hydrogen bond and the decoupling

221   of the H motions shifts the corresponding band to 3441 cm^{-1}.

222   The first protonated M2 vacancy (V_{M2}_O1_O4) is 0.47 eV less stable than

223   V_{M3}_O1_O1 (Table 1). When a M2 vacancy is created, the first proton necessarily goes

224   to the O1 oxygen that is significantly underbonded compared to others. This proton

225   points toward the centre of the vacancy and undergoes repulsion from the second proton.

226   Therefore the corresponding band at 3431 cm^{-1} displays a polarization in the *ac* plane

227   (Fig. 3). The second proton is close to the O4-O4 octahedral edge, and with a long O4-H

228   bond (1.017 Å) leads to a band at 2909 cm^{-1} polarized along the *b*-axis.

229   Finally, the OH-defect corresponding to the building block of the most common

230   structural model for hydrous wadsleyite (Smyth 1994) is found to be less favorable

231   energetically (i.e. V_{M2}_O1_O1 is 0.69 eV less stable than V_{M3}_O1_O1). The two O1-H

232   groups are aligned along the *c*-axis with no obvious hydrogen bond (Fig. 3). One points

233   toward the centre of the M2 vacancy (3454 cm^{-1}) while the other points toward the centre

234   of a normally vacant octahedral site (3515 cm^{-1}). This OH-defect corresponds to the one

235   considered for wadsleyite in the theoretical studies of Winkler et al. (1995) and Balan et

236   al. (2008).

237

238   **4.2. Hydrogarnet-type OH-defects**

239   In wadsleyite, all silicon sites are equivalent. In the case of a silicon vacancy, a

240   bond valence analysis (Donnay and Allmann 1970) indicates the following residual

241   valences 0.96, 1.00 and 1.22 v.u. for the O3, the two O4 and the O2 oxygens,

242   respectively. Seven starting configurations are investigated. All optimized configurations

243   are similar in energy, within 0.1 eV. The two most favorable are shown in Fig. 4 and

244   Table 2.

245       $V_{Si}A$ OH-defect can be described as a cycle O4…O3…O4 where each oxygen

246   atom is donor and acceptor of proton. The fourth proton bound to the O2 oxygen points

247   toward a O4 oxygen. The corresponding spectrum displays four bands. The band at the

248   lowest wavenumber (3409 cm^{-1}) and with contributions in the three directions is related

249   to the longest group, O2-H. The O4-H…O4 bond is parallel to the *a*-axis and corresponds

11

250   to the band at 3550 cm^{-1}. The two other groups, O4-H and O3-H, lead to a doublet at

251   higher wavenumber, 3673 and 3708 cm^{-1}, that are mainly polarized along the *a* and *c*-

252   axis, respectively.

253   In the second hydrogarnet-type defect, $V_{Si}B$, the cycle O4…O3…O4 is also

254   present, leading to the same polarization of the three highest absorption bands. Because

255   of slightly shorter OH bonds, these three bands are observed between 3701 and 3798 cm^{-}

256   ^{1}. The main difference with respect to the $V_{Si}A$ defect is the O2-H group, which switches

257   from the O4 oxygen to the O2 oxygen. This latter OH group corresponds to the band at

258   3375 cm^{-1} polarized along the *a* axis. It must also be noticed that because of the similar

259   stability of these two OH-defects, $V_{Si}B$ configuration is not retained at high-pressure and

260   turns back to a $V_{Si}A$ configuration.

261

262   **4.3. Silicon vacancies compensated by a magnesium cation and two protons**

263   This type of OH-defects involving more complex charge-compensating

264   mechanisms has already been invoked in other nominally anhydrous minerals (e.g.

265   Blanchard et al. 2009, Balan et al. 2012, Panero 2010). Here the magnesium cation is

266   placed either in the vacant tetrahedral site or in a normally vacant octahedral sites

267   adjacent to the silicon vacancy. In other words, magnesium is in interstitial site. Eight

268   starting configurations are investigated. The most stable configuration found corresponds

269   to the situation where the extra magnesium is located outside the silicon vacancy

270   ($V_{Si}\_M_i$) but the relative stabilization of this defect is small. All optimized OH-defects

271   are within 0.28 eV. In this $V_{Si}\_M_i$ defect as well as in the defect with magnesium in

272   silicon vacancy (M_{Si}), the same oxygens, O3 and O4, are protonated (Fig. 5 and Table 3).

12

273   The orientation of the OH groups is however very different leading to contrasted IR

274   spectra. In $V_{Si}\_M_i$, the O4-H group points toward the O3 oxygen and the O3-H group

275   points toward the other O4 oxygen of the vacancy. This leads to the bands at 3468 and

276   3541 cm^{-1}, respectively, with components in the three directions. A small coupling of

277   hydrogen motions explains why the high-wavenumber band is more intense than the

278   other, in contrast with the general relation between OH absorption coefficients and

279   wavenumber (e.g. Libowitzky and Rossman 1997). This general relation relies on the fact

280   that in the case of OH-stretching modes, the IR absorptivity is directly related to the

281   magnitude of the hydrogen Born effective charge along the OH bond (Balan et al. 2008).

282   In the M_{Si} defect, the vacancy being occupied by the magnesium cation, the O3-H group

283   points toward the O3 oxygen of another Si_2O_7 group giving rise to the band at 2995 cm^{-1},

284   mainly polarized along the *a*-axis. The O4-H group is mainly oriented along the *b*-axis

285   with a non-linear hydrogen bond (O4-H...O4 angle ~ 135°) that leads to a IR band at

286   3301 cm^{-1}.

287

288   **4.4. OH-defects associated with the migration of a silicon cation**

289   In line with the interpretation of Kudoh and Inoue (1999) about the partial

290   occupancy by silicon of a normally vacant tetrahedral site (Si2), we consider a last type

291   of OH-defects formed by a silicon cation displaced from its site to the Si2 site adjacent to

292   either one or two magnesium vacancies in M3 site. Two or four protons are needed to

293   compensate the charge and must be bound to the oxygen atoms of the silicon and/or

294   magnesium vacancies. In contrast, the model of Smyth et al. (1997) assuming that the Si2

295   silicon cation comes from a M3 site, does not necessitate protons to compensate the

13

296   charge, which would be balanced instead by an extra magnesium vacancy or a

297   magnesium cation in silicon site. In our case, bond valence analysis evidences that the

298   most underbonded oxygen atoms are the O3 of silicon vacancy followed equally by the

299   O2 of the silicon vacancy and the O1 of the magnesium vacancies. Calculations confirm

300   this trend. The defect with only one magnesium vacancy ($V_{Si}\_Si2\_V_{M3}$) is formed by a

301   O3-H group pointing toward the centre of the silicon vacancy and a O1-H group pointing

302   toward the apical O4 oxygen of the magnesium vacancy (Fig. 6 and Table 4). The O3-H

303   group with no obvious hydrogen bond leads to an absorption band at 3711 cm^{-1} that is

304   polarized in the *bc* plane, and the O1-H group is related to the band at 3365 cm^{-1}. In the

305   case with two magnesium vacancies, another O1-H group is present in the second

306   magnesium vacancy. Their hydrogen motions are coupled in in-phase and out-of-phase

307   stretching vibrations, giving rise to the overlapped bands at 3372 and 3377 cm^{-1}. The

308   fourth hydrogen protonates the O2 oxygen of the silicon vacancy and points toward a O4

309   oxygen, leading to the band at 3245 cm^{-1}. The presence of this fourth hydrogen slightly

310   disturbs the O3-H group and shifts the corresponding band to 3796 cm^{-1} while the

311   polarization is almost unchanged.

312

313   **5. DISCUSSION**

314

315   **5.1. Interpretation of the major group of OH-stretching bands**

316   As described in introduction, the major group of bands is formed by a doublet

317   with bands A and B that have an independent behavior as a function of the water content

318   (Fig. 1). At low water content (~150 wt ppm H_2O), only the band A is visible and is itself

14

319   a thin doublet with a contribution at 3317 cm^{-1} polarized along the *b*-axis and a

320   contribution at 3326 cm^{-1} polarized in the *ac* plane. In addition the band B appears with a

321   minimal pleochroism (slightly more intense along the *c*-axis) in samples containing more

322   than ~3000 wt ppm H_2O (Jacobsen et al. 2005).

323   The OH-defect V_{M3}_O1_O1 is in good agreement with the position and

324   pleochroism of the thin doublet A (Fig. 2), which is therefore assigned to OH groups

325   vibrating along the O1…O4 unshared edges of the M3 octahedron. The calculated

326   pressure derivative of the OH-stretching frequencies (~ -10 cm^{-1}/GPa, Table 1) is also in

327   excellent agreement with the experimental measurements made on a sample containing

328   8000 wt ppm H_2O (~ -9 cm^{-1}/GPa, Deon et al. 2010). Calculations suggest that the same

329   O1-H…O4 group is also responsible for the band B, when it belongs to OH-defects like

330   V_{Si}_Si2_V_{M3} (Fig. 6).

331   This assignment of the major group of bands is in general agreement with

332   previous studies (Kohn et al. 2002, Jacobsen et al. 2005, Walker et al. 2006, Tsuchiya

333   and Tsuchiya 2009, Deon et al. 2010). It corresponds to vacancies in M3 sites

334   compensated by protons located along the O1…O4 edges. Here, we propose a modeling

335   of the OH-stretching IR spectra, which allows us to specify the incorporation

336   mechanisms. It is clearly shown that the evolution of the spectrum as a function of the

337   water content necessarily involves at least two types of well-defined OH-defects.

338

339   **5.2. Interpretation of the minor group of OH-stretching bands**

340   The situation is more complex for the minor group of bands that is made of the

341   band C polarized in the *bc* plane and another band of smaller intensity, band D, polarized

15

342   in the *ac* plane (Fig. 1). Here again these two bands are independent and at low water

343   content, only the band D is present.

344   Experimentally, Jacobsen et al. (2005) assigned this minor doublet to protonation

345   of other edges of a M3 vacancy (i.e. O1…O3 and O1…O1). This assignment that would

346   fit the pleochroic behavior of these bands, has been ruled out by Deon et al. (2010)

347   because it would not reproduce their high wavenumbers and their pressure dependence.

348   Here, calculations show that it is impossible to stabilize OH groups along these

349   octahedral edges. Deon et al. (2010) suggested instead the involvement of a non-linear

350   O1-H…O2 hydrogen bond. The only possibility we found to deviate the O1-H group

351   from the c-axis in a fully protonated M2 vacancy is the V_{M2}_O1_O4 OH-defect (Fig. 3).

352   The polarization is in good agreement with the observed band D, but the V_{M2}_O1_O4

353   defect would also give rise to a band at ~3000 cm^{-1}, polarized along the *b*-axis. This latter

354   band is not observed experimentally since only a contribution along the *a*-axis is present

355   at ~3000 cm^{-1} (Fig. 1).

356   From their theoretical investigation, Walker et al. (2006) would rather assign the

357   observed minor doublet to a partial protonation of silicon vacancies. In the present study,

358   we obtained several configurations for the hydrogarnet-type defects with similar energies,

359   leading to variable IR signatures. One could find bands in the right wavenumber range

360   and a similar pleochroism as the minor doublet (Fig. 4). But hydrogarnet-type defects

361   generate too many bands and more importantly could not explain the independent

362   behavior of the two bands as a function of the water content. That is why partial

363   protonation has been evoked, like for instance when the charge of the silicon vacancy is

364   compensated by a magnesium cation and two protons (Fig. 5). But in this case, the

16

365   models do not display OH-stretching bands with the right polarizations. A partial

366   protonation of the silicon vacancy is also present in the $V_{Si}\_Si2\_V_{M3}$ defect already

367   mentioned for explaining the band B of the major doublet. With such a defect-structure,

368   the O3-H group would lead to a band polarized in the *bc* plane like the observed band C

369   (Fig. 6). With ~ -4 cm^{-1}/GPa for the O3-H group, this OH-defect shows the weakest

370   pressure dependence after the low-wavenuber band of the M_{Si} OH-defect. This is also in

371   agreement with its experimental counterpart that is almost pressure insensitive.

372   The present results thus suggest that the main contribution of the minor doublet

373   (band C) can be interpreted as the partial protonation of a silicon vacancy coupled with

374   the migration of a silicon cation to the normally vacant tetrahedral site (Si2). The less

375   intense contribution (band D) may be related to non-linear O1-H…O2 hydrogen bonds in

376   M2 vacancies, but none of the investigated OH-defects fully satisfies the experimental

377   constraints.

378

379   **5.3. Absorption coefficient of OH-defects in wadsleyite**

380   The quantification of the water content by IR spectroscopy relies on the

381   knowledge of molar absorption coefficients of OH-stretching modes involved. General

382   calibrations have been derived showing a negative relation between the absorption

383   coefficient and the mean wavenumber of the corresponding vibrational mode (Paterson

384   1982, Libowitzky and Rossman 1997). However for nominally anhydrous minerals,

385   mineral-specific calibrations are needed to obtain accurate concentrations (e.g. Balan et

386   al. 2008, Koch-Müller and Rhede 2010). To summarize, the OH-defects that account for

387   the main absorption bands of IR spectra of quenched wadsleyite samples are those

17

388   involving M3 vacancies, i.e. the fully protonated M3 vacancies, $V_{M3}\_O1\_O1$, and OH-

389   defects associated with the migration of a silicon cation, $V_{Si}\_Si2\_V_{M3}$ and $V_{Si}\_Si2\_2V_{M3}$.

390   Only the theoretical integrated molar absorption coefficients of these likely OH-defects

391   are reported in Figure 7a. We can distinguish two sets of data, one for 0 GPa and the

392   other for 15 GPa. As already pointed out in Blanchard et al. (2009) for ringwoodite, the

393   evolution of the wavenumber and the absorption coefficient with pressure depends on the

394   local environment of the OH group but globally absorption coefficients increase with

395   pressure while the average wavenumbers decrease. The distinction of two data sets means

396   that for a precise quantification of the hydrogen content in *in situ* experiments, one must

397   consider a higher absorption coefficient than the one determined after quench at 0 GPa

398   (Deon et al. 2010).

399   Absorption coefficients of OH-defects in forsterite and ringwoodite have already

400   been computed using the same theoretical method (Blanchard et al. 2009, Balan et al.

401   2011). We can then compile the theoretical data for the three Mg_2SiO_4 polymorphs,

402   considering only the most-likely OH-defects at 0 GPa (Fig. 7b). In agreement with

403   experimental studies (Thomas et al. 2009, Koch-Müller et al. 2010, Withers et al. 2012),

404   we find that all data are below the general theoretical trend derived by Balan et al. (2008)

405   using mainly hydrous minerals. Considering the small number of data points for each

406   mineral and considering the relatively small data scattering, it is possible to fit the whole

407   data of the three polymorphs by the single following relation: $K_{int} = 278.7\pm18.1$

408   ($3810\pm465 - x$). This trend suggests that an absorption coefficient obtained from a general

409   calibration would underestimate the water content of the Mg_2SiO_4 minerals. This

410   underestimation depends on the position of the main absorption bands. It is almost

18

411   negligible for wavenumbers around 3600 cm^{-1}, but becomes important for smaller

412   wavenumbers. For instance for the major band of wadsleyite, observed at ~3350 cm^{-1}, the

413   absorption coefficient obtained from the Mg_2SiO_4 calibration is ~23 % lower than the one

414   obtained from the general calibration. This is consistent with the experimental

415   determination by Deon et al. (2010) of an integrated molar absorption coefficient of 73

416   000 cm^{-2} per mol H_2O/L that is well below the general calibration curves. For instance,

417   the calibration of Libowitzky and Rossman (1997) gives an absorption coefficient of 91

418   512 cm^{-2} per mol H_2O/L (~25 % higher) for the same wavenumber. To compare the three

419   Mg_2SiO_4 polymorphs, one must keep in mind the positions of the main absorption bands

420   in each mineral. For the range of the main absorption bands in wadsleyite (~ 3350 cm^{-1})

421   and ringwoodite (~ 3150 cm^{-1}), the calculated absorption coefficient for ringwoodite is 44

422   % larger than the one for wadsleyite, which is in good agreement with the results of

423   Koch-Müller et al. (2010) who obtained an absorption coefficient for the Mg end-

424   member of ringwoodite 43 % larger than the wadsleyite value of Deon et al. (2010).

425   Forsterite displays a large variety of OH-stretching IR spectra with bands ranging from

426   3200 to 3650 cm^{-1}. For IR spectra dominated by high-frequency bands, Thomas et al.

427   (2009) and Withers et al. (2012) found absorption coefficients between 35 000 and 50

428   000 cm^{-2} per mol H_2O/L that is significantly lower than the wadsleyite coefficient of Deon

429   et al. (2010), i.e. 73 000 cm^{-2} per mol H_2O/L. All these trends are supported by our

430   theoretical results (Fig. 8). It is also interesting to note that the relation between the OH

431   bond length and the stretching wavenumber determined for forsterite, ringwoodite and

432   enstatite (Balan et al. 2012) also apply to wadsleyite.

19

433   In conclusion, a specific calibration for the Mg_2SiO_4 polymorphs must be used to

434   quantify accurately the water content of these minerals from IR spectroscopy. Results

435   also suggest that the calibration determined at 0 GPa from quenched samples does not

436   apply with the same accuracy to *in situ* IR measurements.

437

438   **5.4. Concluding remarks about the bands assignment**

439   Jacobsen et al. (2005) pointed out that the *b/a* axial ratio of wadsleyite increases

440   with increasing water content. Figure 8 shows this empirical relation as well as the

441   calculated OH-defects. All OH-defects involving M3 vacancies and proposed here to

442   interpret the IR spectra, follow a similar trend as the one seen experimentally (i.e. the

443   fully protonated M3 vacancies, $V_{M3}\_O1\_O1$, and OH-defects associated with the

444   migration of a silicon cation, $V_{Si}\_Si2\_V_{M3}$ and $V_{Si}\_Si2\_2V_{M3}$). Note that the $V_{M3}\_O1\_O3$

445   defect, which falls in the right range, was ruled out because of its relative energy with

446   respect to the $V_{M3}\_O1\_O1$ defect (0.37 eV less stable). On the other hand, the protonated

447   M2 vacancies lead to a smaller *b/a* ratio than that observed for anhydrous wadsleyite and

448   the creation of the hydrogarnet-type defects does not change much the axial ratio.

449   Based on results inferred from X-ray diffraction studies and from the

450   confrontation of experimental and theoretical IR spectra, we propose the following

451   mechanisms of hydrogen incorporation in wadsleyite. At low water content, protons are

452   associated with M3 vacancies, thus forming preferentially $V_{M3}\_O1\_O1$ OH-defects,

453   which are the energetically most favorable OH-defects. This yields the thin doublet A

454   (Fig. 1a). In addition, the small band D indicates that a small amount of non-linear O1-

455   H...O2 hydrogen bonds is formed in M2 vacancies. As experimentally seen, the number

20

456 of M3 vacancies increases with the water content. More V_{M3}_O1_O1 OH-defects are

457 formed. The high concentration of M3 vacancies facilitates the migration of silicon cation

458 to Si2 sites that is accompanied by a redistribution of protons. This leads to the formation

459 of OH-defects like V_{Si}_Si2_V_{M3} and V_{Si}_Si2_2V_{M3} that are responsible of the absorption

460 bands B and C (Fig. 1b). Other OH-defects may also be involved in a smaller extent as

461 reflected by the additional weak bands observed in wadsleyite spectra.

462   If the migration of silicon cation to Si2 sites occurs during the decompression, as

463 suggested by Smyth et al. (1997) and Kudoh and Inoue (1999), it means that the IR

464 spectra collected at 0 GPa and even the high-pressure IR spectra collected on quenched

465 samples do not reflect the population of OH-defects present in mantle conditions. In this

466 case, calculations predict that the wadsleyite IR spectra would be dominated by the main

467 group of absorption bands reported around 3350 cm^{-1} at 0 GPa (these bands would be

468 shifted to lower wavenumbers under pressure), and associated with fully protonated M3

469 vacancies. IR spectra collected *in situ* and during the sample decompression would allow

470 tackling this question.

471

474

21

References

475 Balan, E., Lazzeri, M., Saitta, A.M., Allard, T., Fuchs, Y., and Mauri, F. (2005) First-
477 principles study of OH stretching modes in kaolinite, dickite and nacrite.
478 American Mineralogist, 90, 50-60.

479 Balan, E., Lazzeri, M., Delattre, S., Méheut, M., Refson, K., and Winkler, B. (2007)
480 Anharmonicity of inner-OH stretching modes in hydrous phyllosilicates:
481 assessment from first-principles frozen-phonon calculations. Physics and
482 Chemistry of Minerals, 34, 621–625.

483 Balan, E., Refson, K., Blanchard, M., Delattre, S., Lazzeri, M., Ingrin, J., Mauri, F.,
484 Wright, K., and Winkler, B. (2008) Theoretical infrared absorption coefficient of
485 OH groups in minerals. American Mineralogist, 93, 950-953.

486 Balan, E., Ingrin, J., Delattre, S., Kovacs, I., and Blanchard, M. (2011) Theoretical
487 infrared spectrum of OH-defects in forsterite. European Journal of Mineralogy,
488 23, 285-292.

489 Balan, E., Blanchard, M., Yi, H., and Ingrin, J. (2013) Theoretical study of OH-defects
490 in pure enstatite. Physics and Chemistry of Minerals, 40, 41-50.

491 Baroni, S., de Gironcoli, S., Dal Corso, A., and Giannozzi, P. (2001) Phonons and related
492 crystal properties from density-functional perturbation theory. Reviews of
493 Modern Physics, 73, 515-561.

494 Blanchard, M., Balan, E., and Wrigth, K. (2009) Incorporation of water in iron-free
495 ringwoodite: a first-principles study. American Mineralogist, 94, 83-89.

496 Bolfan-Casanova, N., Keppler, H., and Rubie, D.C. (2000) Water partitioning between
497 nominally anhydrous minerals in the MgO-SiO_2-H_2O system up to 24 GPa:

498   implications for the distribution of water in the Earth's mantle. Earth and

499   Planetary Science Letters, 182, 209-221.

500 Demouchy, S., Deloule, E., Frost, D.J., and Keppler, H. (2005) Pressure and temperature-

501   dependence of water solubility in Fe-free wadsleyite. American Mineralogist, 90,

502   1084-1091.

503 Deon, F., Koch-Müller, M., Rhede, D., Gottschalk, M., Wirth, R., and Thomas, S.-M.

504   (2010) Location and quantification of hydroxyl in wadsleyite: New insights.

505   American Mineralogist, 95, 312-322.

506 Donnay, G. and Allmann, R. (1970) How to recognize O^{2-}, OH^-, and H_2O in crystal

507   structures determined by X-rays. American Mineralogist, 55, 1003-1015.

508 Finocchi, F., Hacquart, R., Naud, C., and Jupille, J. (2008) Hydroxyl-defect complexes

509   on hydrated MgO smokes. Journal of Physical Chemistry, 112, 13226-13231.

510 Giannozzi, P., Baroni, S., Bonini, N., Calandra, M., Car, R., Cavazzoni, C., Ceresoli, D.,

511   Chiarotti, G.L., Cococcioni, M., Dabo, I., Dal Corso, A., de Gironcoli, S., Fabris,

512   S., Fratesi, G., Gebauer, R., Gerstmann, U., Gougoussis, C., Kokalj, A., Lazzeri,

513   M., Martin-Samos, L., Marzari, N., Mauri, F., Mazzarello, R., Paolini, S.,

514   Pasquarello, A., Paulatto, L., Sbraccia, C., Scandolo, S., Sclauzero, G., Seitsonen,

515   A.P., Smogunov, A., Umari, P., and Wentzcovitch, R.M. (2009) Quantum

516   ESPRESSO: a modular and open-source software project for quantum simulations

517   of materials. Journal of Physics: Condensed Matter, 21, 395502.

518 Haiber, M., Ballone, P., and Parrinello, M. (1997) Structure and dynamics of protonated

519   Mg_2SiO_4: An ab-initio molecular dynamics study. American Mineralogist, 82,

520   913-922.

23

521   Horiuchi, H. and Sawamoto, H. (1981) β-Mg_2SiO_4: Single-crystal X-ray diffraction

522   study. American Mineralogist, 66, 568-575.

523   Inoue, T., Yurimoto, H., and Kudoh, Y. (1995) Hydrous modified spinel

524         $Mg_{(1.75)}SiH_{(0.5)}O_4$: A new water reservoir in the mantle transition zone. American

525   Mineralogist, 22, 117-120.

526   Jacobsen, S.D., Demouchy, S., Frost, D.J., Boffa Ballaran, T., and Kung, J. (2005) A

527   systematic study of OH in hydrous wadsleyite from polarized FTIR spectroscopy

528   and single-crystal X-ray diffraction: Oxygen sites for hydrogen storage in Earth's

529   interior. American Mineralogist, 90, 61-70.

530   Keppler, H. and Smyth, J.R., eds (2006) Water in nominally anhydrous minerals, vol. 62

531   of Reviews in Mineralogy and Geochemistry (Geophysical Society and

532   Mineralogical Society of America, Chantilly, Virginia, USA).

533   Kleppe, A.K., Jephcoat, A.P., Olijnyk, H., Slesinger, A.E., Kohn, S.C., and Wood, B.J.

534   (2001) Raman spectroscopic study of hydrous wadsleyite (β-Mg_2SiO_4) to 50 GPa.

535   Physics and Chemistry of Minerals, 28, 232-241.

536   Koch-Müller, M. and Rhede, D. (2010) IR absorption coefficients for water in nominally

537   anhydrous high-pressure minerals. American Mineralogist, 95, 770-775.

538   Kohlstedt, D.L., Keppler, H., and Rubie, D.C. (1996) Solubility of water in the α, β, and

539   γ phases of $(Mg,Fe)_2SiO_4$. Contributions to Mineralogy and Petrology, 123, 345-

540   357.

541   Kohn, S.C., Brooker, R.A., Frost, D.J., Slesinger, A.E., and Wood B.J. (2002) Ordering

542   of hydroxyl defects in hydrous wadsleyite (β-Mg_2SiO_4). American Mineralogist,

543   87, 293-301.

24

544 Libowitzky, E. and Rossman, G.R. (1997) An IR absorption calibration for water in

545   minerals. American Mineralogist, 82, 1111-1115.

546 McMillan, P.F., Akaogi, M., Sato, R.K., Poe, B., and Foley, J. (1991) Hydroxyl groups in

547   β-Mg$_2$SiO$_4$. American Mineralogist, 76, 354-360.

548 Monkhorst, H.J. and Pack, J.D. (1976) Special points for Brillouin-zone integrations.

549   Physical Review B, 13, 5188-5192.

550 Panero, W. (2010) First principles determination of the structure and elasticity of hydrous

551   ringwoodite. Journal of Geophysical Research, 115, B03203.

552 Parker, S.C., Cooke, D.J., Kerisit, S., Marmier, A.S., Taylor, S.L., and Taylor, S.N.

553   (2004) From HADES to PARADISE—atomic simulation of defects in minerals.

554   Journal of Physics: Condensed Matter, 16, S2735-S2749.

555 Paterson, M.S. (1982) The determination of hydroxyl by infrared absorption in quartz,

556   silicate glasses and similar materials. Bulletin de Minéralogie, 105, 20-29.

557 Perdew, J.P., Burke, K., and Ernzerhof, M. (1996) Generalized Gradient Approximation

558   Made Simple. Physical Review Letters, 77, 3865–3868.

559 Ross, N.L., Gibbs, G.V., and Rosso, K.M. (2003) Potential docking sites and positions of

560   hydrogen in high-pressure silicates. American Mineralogist, 88, 1452-1459.

561 Smyth, J.R. (1987) β-Mg$_2$SiO$_4$: A potential host for water in the mantle? American

562   Mineralogist, 72, 1051-1055.

563 Smyth, J.R. (1994) A crystallographic model for hydrous wadsleyite (β-Mg$_2$SiO$_4$): An

564   ocean in the Earth's interior? American Mineralogist, 79, 1021-1024.

565   Thomas, S.M., Koch-Müller, M., Reichart, P., Rhede, D., Thomas, R., Wirth, R., and

566   Matsyuk, S. (2009) IR calibrations for water determination in olivine, r-GeO$_2$, and

567   SiO$_2$ polymorphs. Physics and Chemistry of Minerals, 36, 489-509.

568   Tsuchiya, J. and Tsuchiya, T. (2009) First principles investigation of the structural and

569   elastic properties of hydrous wadsleyite under pressure. Journal of Geophysical

570   Research, 114, B02206.

571   Verma, A.K. and Karki, B.B. (2009) Ab initio investigations of native and protonic point

572   defects in Mg$_2$SiO$_4$ polymorphs under high pressure. Earth's mantle. Earth and

573   Planetary Science Letters, 285, 140-149.

574   Walker, A.M., Demouchy, S., and Wrigth, K. (2006) Computer modeling of the

575   energeties and vibrational properties of hydroxyl groups in α- and β-Mg$_2$SiO$_4$.

576   European Journal of Mineralogy, 18, 529-543.

577   Winkler, B., Milman, V., Hennion, B., Payne, M.C., Lee, M.-H., and Lin, J.S. (1995) Ab

578   initio total energy study of brucite, diaspora and hypothetical hydrous wadsleyite.

579   Physics and Chemistry of Minerals, 22, 461-467.

580   Withers, A.C., Bureau, H., Raepsaet, C., and Hirschmann, M.M. (2012) Calibration of

581   infrared spectroscopy by elastic recoil detection analysis of H in synthetic olivine.

582   Chemical Geology, 334, 92-98.

583   Wright, K. and Catlow, C.R.A. (1996) Calculations on the energetics of water dissolution

584   in wadsleyite. Physics and Chemistry of Minerals, 23, 38-41.

585   Ye, Y., Smyth, J.R., Hushur, A., Manghnani, M.H., Lonappan, D., Dera, P., and Frost,

586   D.J. (2010) Crystal structure of hydrous wadsleyite with 2.8% H$_2$0 and

587   compressibility to 60 GPa. American Mineralogist, 95, 1765-1772.

588   Young, T.E., Green, II H.W., Hofmeister, A.M., and Walker, D. (1993) Infrared

589   spectroscopic investigation of hydroxyl in β-Mg_2SiO_4 and coexisting olivine:

590   Implications for mantle evolution and dynamics. Physics and Chemistry of

591   Minerals, 19, 409-422.

592

593   **Figure Captions**

594

595   **Figure 1.** Polarized IR spectra of synthetic hydrous wadsleyite (after Jacobsen et al.

596   2005)

597

598   **Figure 2.** Structural models and theoretical polarized IR spectra of protonated Mg

599   vacancies at the M3 site (referred as $V_{M3}\_O1\_O1$ and $V_{M3}\_O1\_O3$). The position of the

600   main experimental bands (Jacobsen et al. 2005) is reported as dotted lines. X, Y and Z

601   stand for polarization directions along *a*, *b* and *c*-axis, respectively.

602

603   **Figure 3.** Structural models and theoretical polarized IR spectra of protonated Mg

604   vacancies at the M2 site (referred as $V_{M2}\_O1\_O4$ and $V_{M2}\_O1\_O1$).

605

606   **Figure 4.** Structural models and theoretical polarized IR spectra of protonated Si

607   vacancies (referred as $V_{Si}A$ and $V_{Si}B$).

608

609   **Figure 5.** Structural models and theoretical polarized IR spectra of Si vacancies

610   compensated by a magnesium cation and two protons either in interstitial site (referred as

611     $V_{Si}\_M_i$) or in the vacant tetrahedral site (referred as M_{Si}).

612

613   **Figure 6.** Structural models and theoretical polarized IR spectra of OH-defects formed by

614   a silicon cation moved from its site to a normally vacant tetrahedral site (Si2) adjacent to

28

615   either one or two magnesium vacancies in M3 site (referred as $V_{Si}\_Si2\_V_{M3}$ and

616    $V_{Si}\_Si2\_2V_{M3}$).

617

618   **Figure 7.** a. Theoretical integrated molar absorption coefficients of the stretching modes

619   of OH-defects in wadsleyite as a function of their average wavenumber. Circles and

620   squares represent the likely OH-defects in wadsleyite at 0 and 15 GPa, respectively. The

621   general theoretical trend of Balan et al. (2008) is also reported for comparison. b. Same

622   graph for the likely OH-defects in forsterite, triangles (Balan et al. 2011), in wadsleyite at

623   0 GPa, circles (this study) and in ringwoodite at 0 GPa, squares (Blanchard et al. 2009).

624   A single linear fit for the three Mg_2SiO_4 polymorphs leads to the following equation: K_{int}

625    $= 278.7 \pm 18.1 \ (3810 \pm 465 - x)$.

626

627   **Figure 8.** Variation of the (b/a) axial ratio of wadsleyite (at 0 GPa) with water content.

628   Solid square is for anhydrous wadsleyite. The bold line corresponds to the empirical

629   relation derived by Jacobsen et al. (2005), $(b/a) = 2.008(1) + 1.25(3) \times 10^{-6} \cdot C_{H_2O}$.

630

29

631 **TABLES**

632

633 **Table 1**. Properties of protonated Mg vacancies

	a, b, c (Å)[a]	Relative energy (eV)	Integrated molar absorption coefficient (L mol^{-1} cm^{-2})	Bond geometry	dO-H (Å)	dO...O (Å)	ν (cm^{-1})	dν/dP (cm^{-1}/GPa)
V_{M3}_O1_O1	5.688 11.472 8.237	0.0	128850	O1-H...O4	0.990	3.025	3367	-10.0
				O1-H...O4	0.990	3.026	3374	-10.0
V_{M3}_O1_O3	5.676 11.480 8.268	0.37	190489	O3-H...O3	1.022	2.675	2837	-8.6
				O1-H...O4	0.988	3.128	3441	-4.9
V_{M2}_O1_O4	5.714 11.417 8.251	0.47	168762	O4-H...O4	1.017	2.718	2909	-19.9
				O1-H[b]	0.989	—	3431	-5.2
V_{M2}_O1_O1	5.713 11.442 8.241	0.69	55099	O1-H[b]	0.988	—	3454	-3.6
				O1-H[b]	0.987	—	3515	-2.6

634 [a] Dimensions of the 2×1×1 supercell are converted in unit-cell parameters.

635 [b] No obvious single hydrogen bond.

30

636 **Table 2**. Properties of hydrogarnet-type protonated Si vacancies

	a, b, c (Å)[a]	Relative energy (eV)	Integrated molar absorption coefficient (L mol^{-1} cm^{-2})	Bond geometry	dO-H (Å)	dO...O (Å)	ν (cm^{-1})	dν/dP (cm^{-1}/GPa)
V$_{Si}$A	5.701	0.0	85800	O2-H...O4	0.986	2.800	3409	-8.1
	11.499			O4-H...O4	0.979	2.995	3550	-12.6
	8.262			O4-H...O3	0.972	3.152	3673	-9.1
				O3-H...O4	0.972	3.032	3708	-8.0
V$_{Si}$B	5.704	0.02	70732	O2-H...O2	0.990	2.723	3375	—[b]
	11.487			O4-H...O4	0.971	3.105	3701	—
	8.260			O4-H...O3	0.970	3.174	3746	—
				O3-H...O4	0.967	3.189	3792	—

637   [a] Dimensions of the 2×1×1 supercell are converted in unit-cell parameters.

638   [b] Under pressure, V$_{Si}$B OH-defect turns back to the more stable V$_{Si}$A configuration.

639

640

641

642

643

644

645

646

647

648

31

649 **Table 3**. Properties of Si vacancies compensated by a magnesium cation and two protons

	a, b, c (Å)[a]	Relative energy (eV)	Integrated molar absorption coefficient (L mol^{-1} cm^{-2})	Bond geometry	dO-H (Å)	dO...O (Å)	ν (cm^{-1})	dv/dP (cm^{-1}/GPa)
$V_{Si}\_M_i$	5.718	0.0	89382	O4-H...O3	0.985	3.076	3468	-19.3
	11.522			O3-H...O4	0.980	3.124	3541	-16.9
	8.245							
M_{Si}	5.710	0.09	174840	O3-H...O3	1.009	2.643	2995	-2.1
	11.513			O4-H...O4[b]	0.994	2.777	3301	-14.1
	8.276							

650 [a] Dimensions of the 2×1×1 supercell are converted in unit-cell parameters.

651 [b] This hydrogen bond is significantly angled (O-H...O angle ~ 135°).

652

653

654

655

656

657

658

659

660

661

32

662   **Table 4**. Properties of OH-defects formed by a silicon cation moved from its site to a

663   normally vacant tetrahedral site (Si2) adjacent to either one or two magnesium vacancies

664   in M3 site

	a, b, c $(\text{Å})^a$	Relative energy (eV)	Integrated molar absorption coefficient (L mol^{-1} cm^{-2})	Bond geometry	dO-H (Å)	dO...O (Å)	ν (cm^{-1})	$d\nu/dP$ (cm^{-1}/GPa)
$V_{Si}\_Si2\_V_{M3}$	5.696	—[b]	88065	O1-H...O4	0.991	3.013	3365	-12.3
	11.500			O3-H [c]	0.972	—	3711	-3.5
	8.267							
$V_{Si}\_Si2\_2V_{M3}$	5.682	—[b]	121972	O2-H...O4	0.996	2.780	3245	-11.5
	11.516			O1-H...O4	0.990	3.028	3372[d]	-12.4
	8.234			O1-H...O4	0.990	3.032	3377[d]	-12.3
				O3-H...O4	0.967	3.243	3796	-4.5

665   [a] Dimensions of the 2×1×1 supercell are converted in unit-cell parameters.

666   [b] The relative energy is not reported since these OH-defects do not have the same

667   stoichiometry.

668   [c] No obvious single hydrogen bond.

669   [d] Modes involving a coupled motion of OH groups.
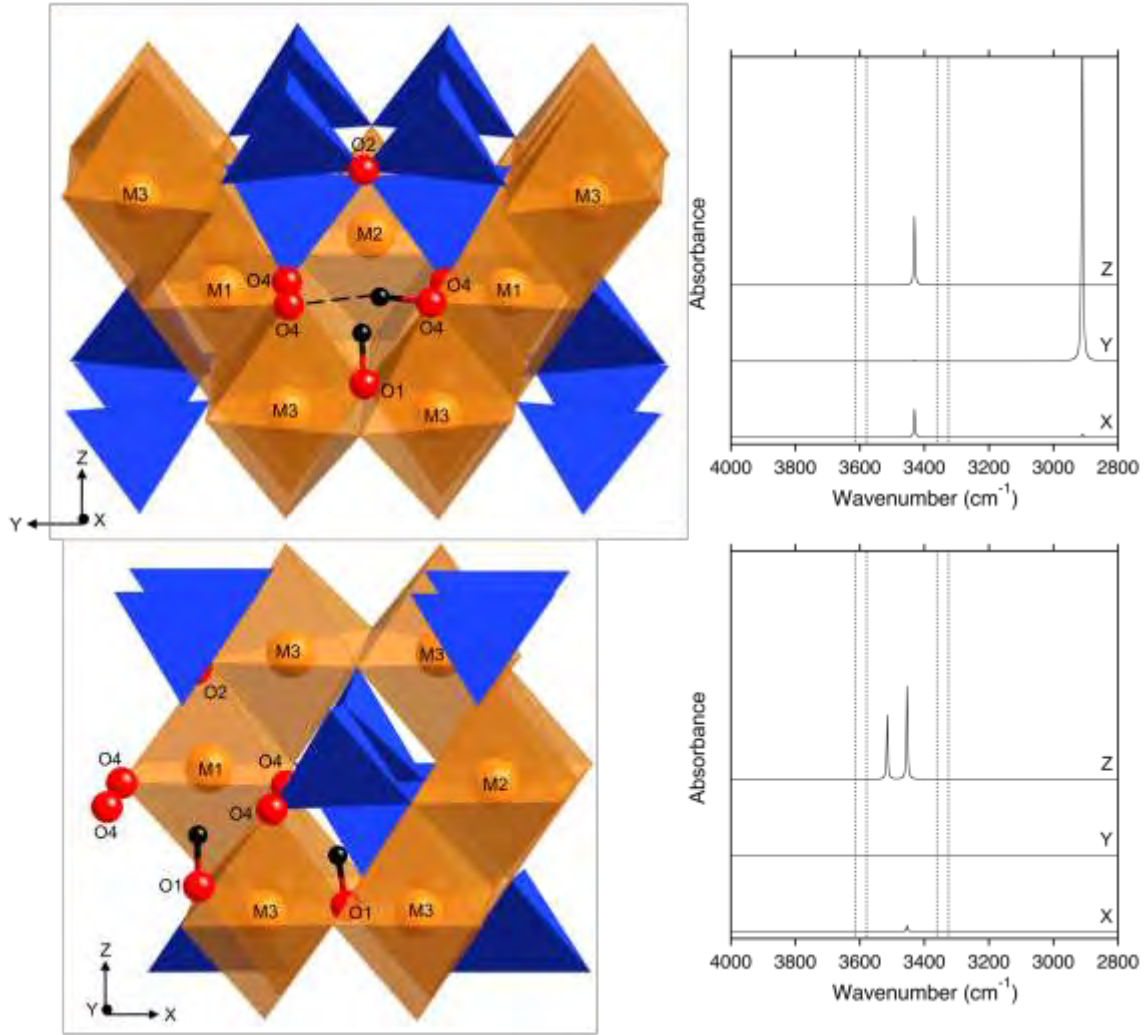
670
671

33

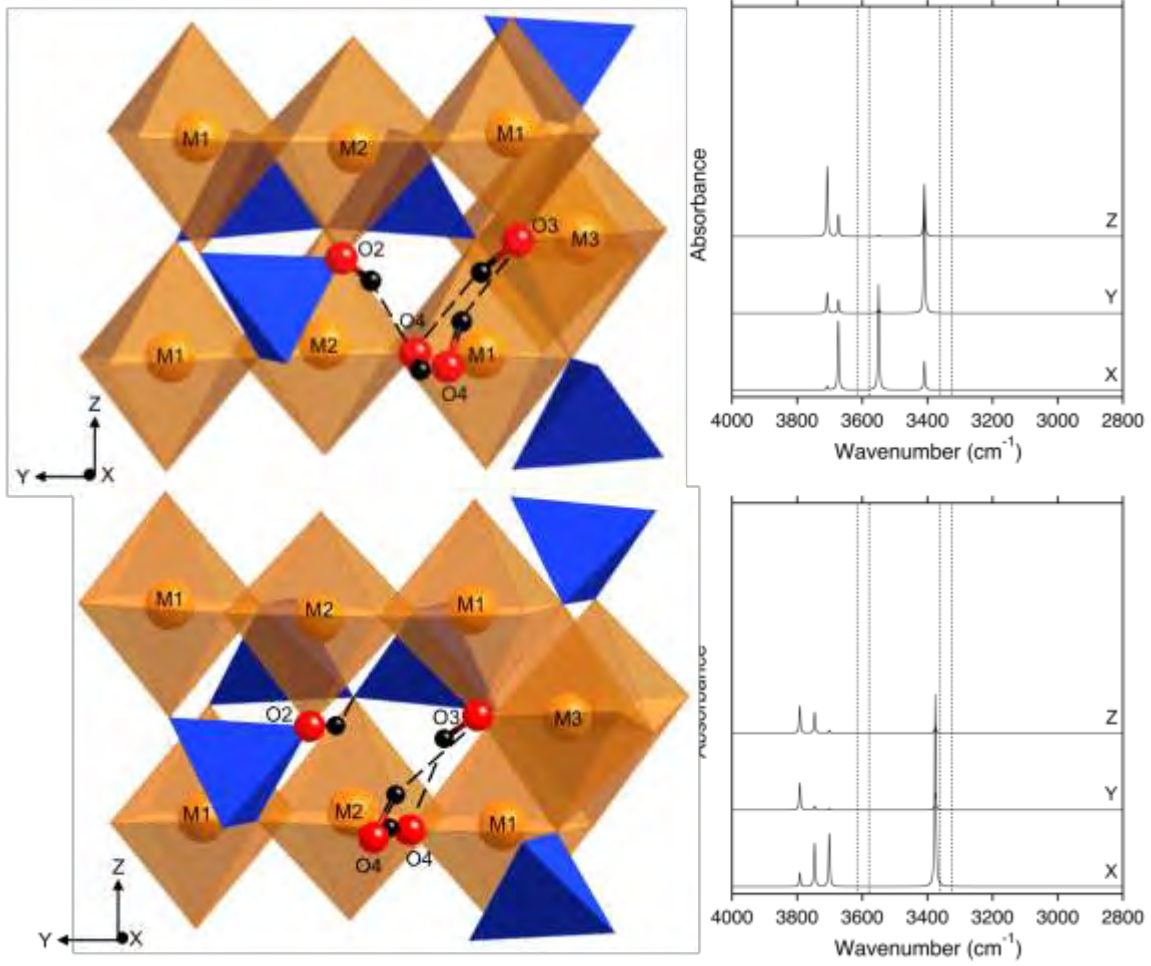672

673   Fig. 1

674

34

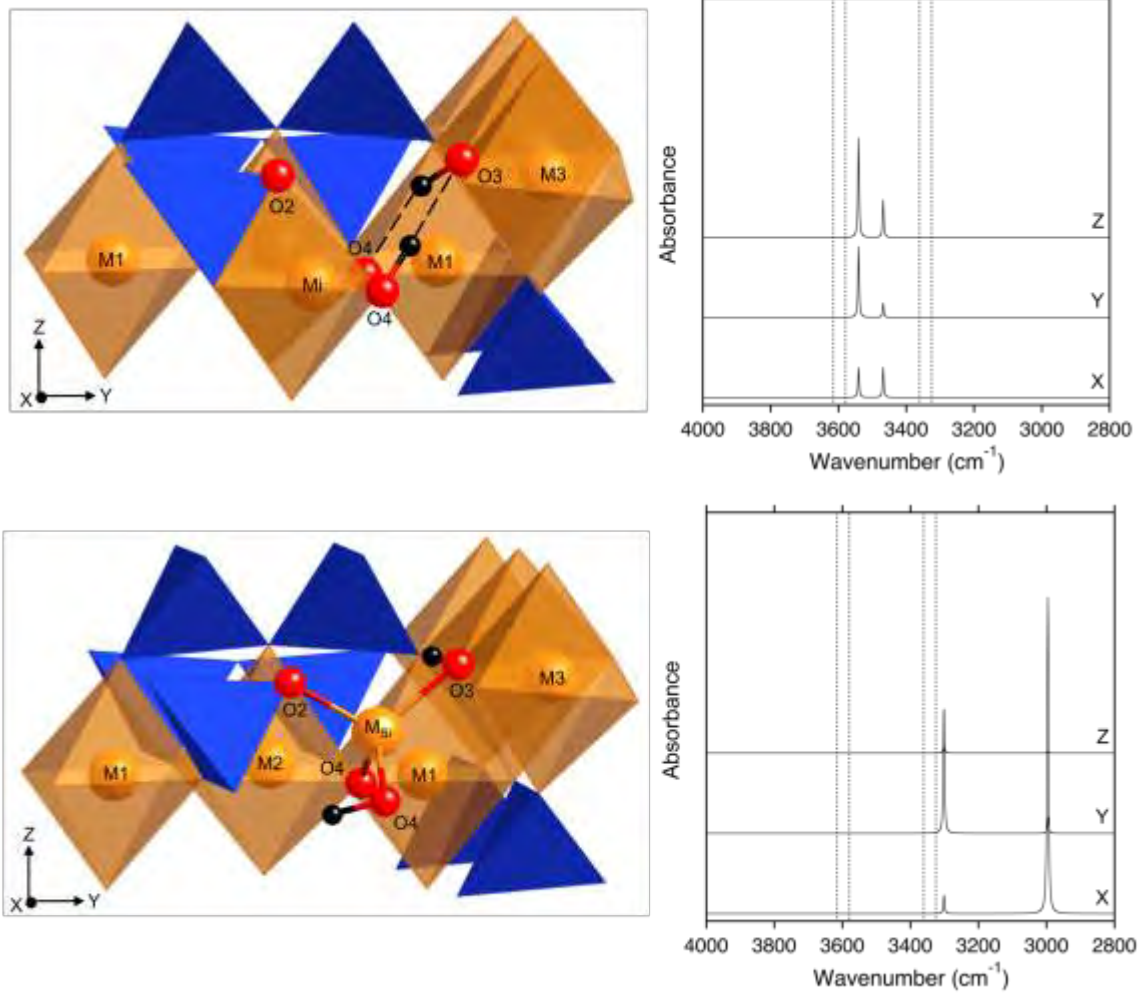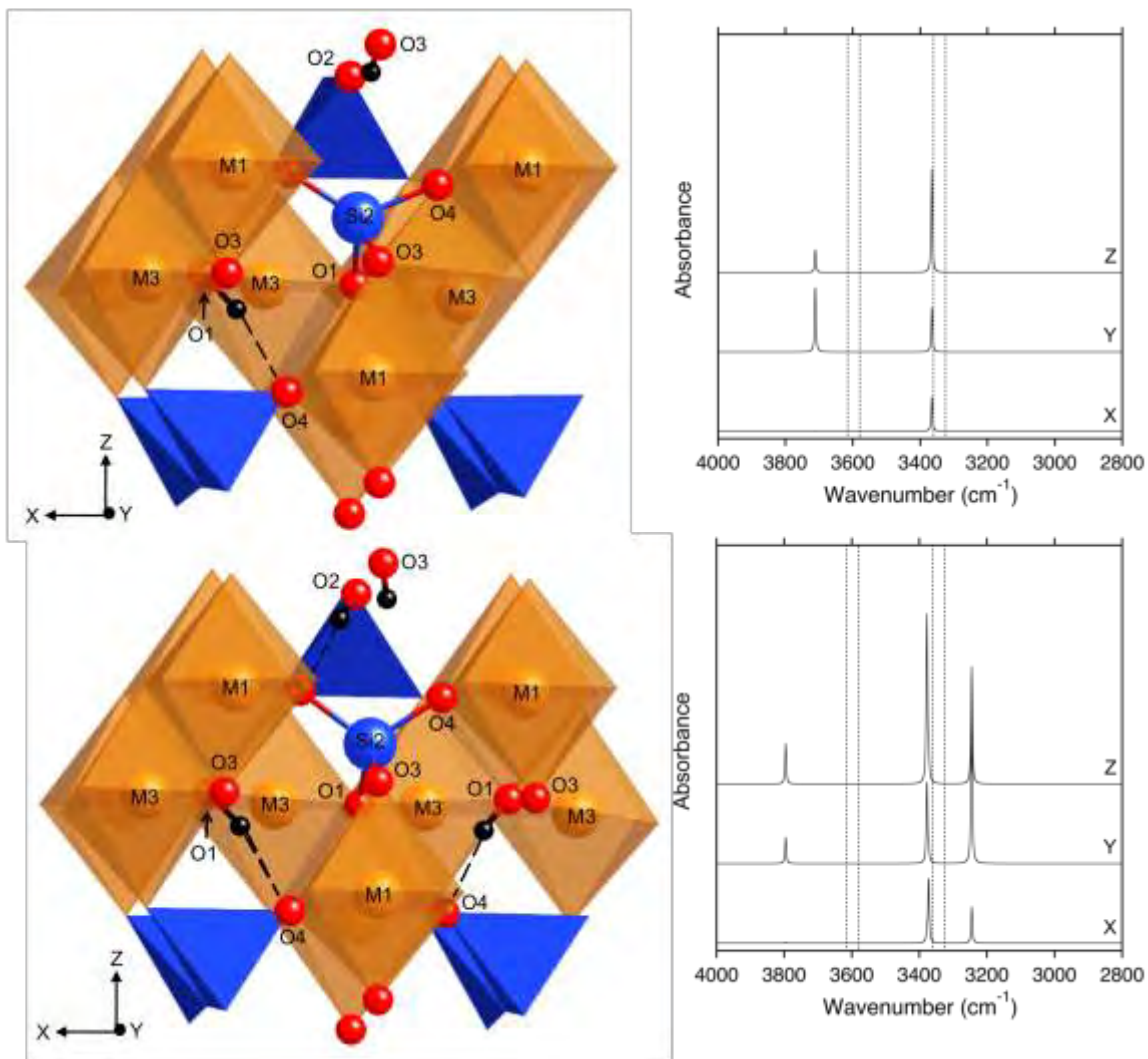675

676   Fig. 2

677

35
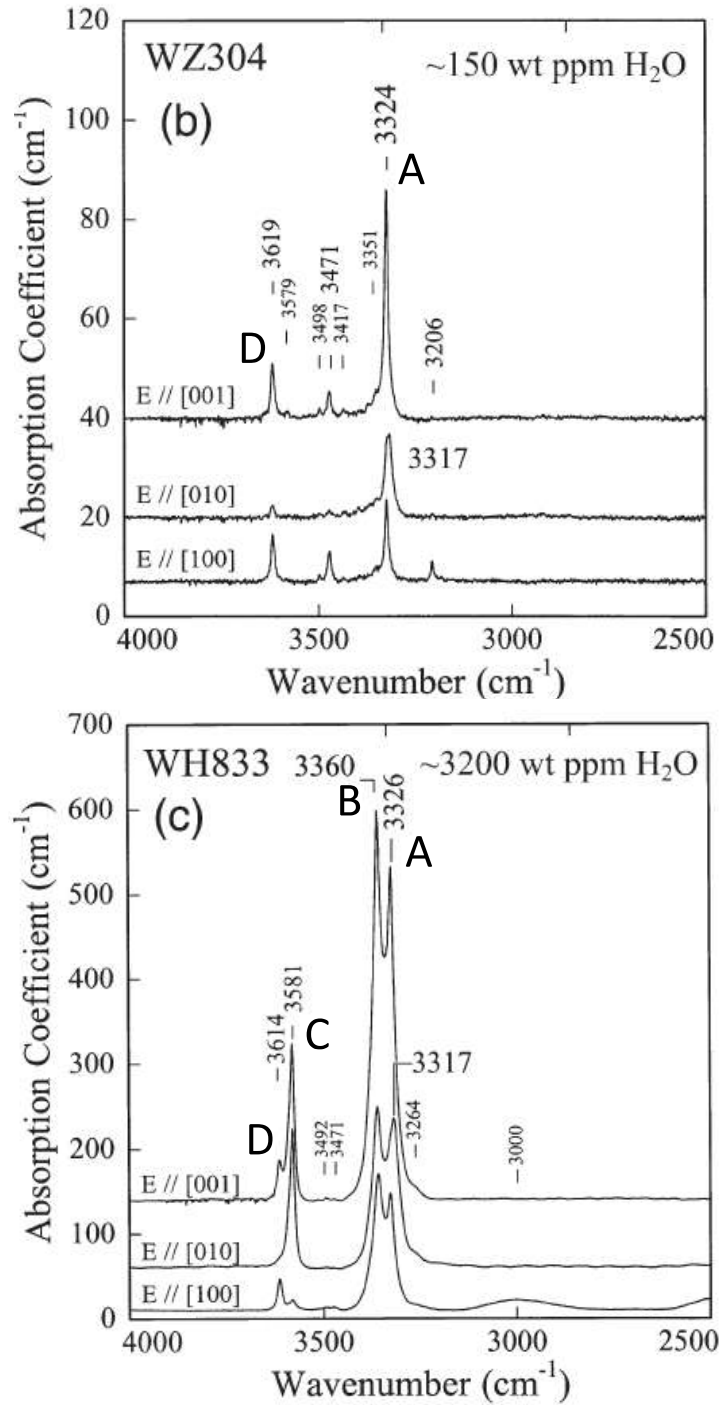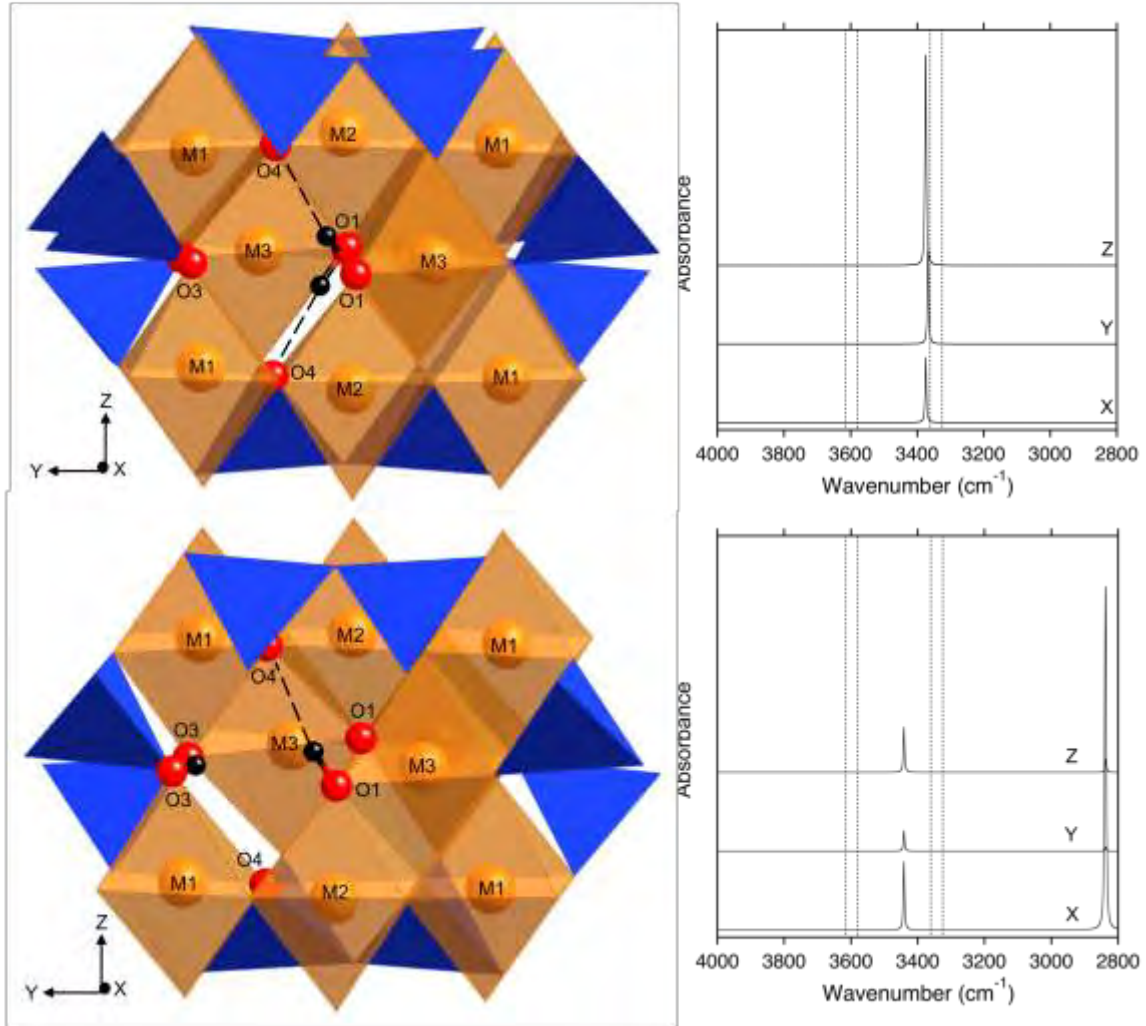
678

679   Fig. 3

680

681

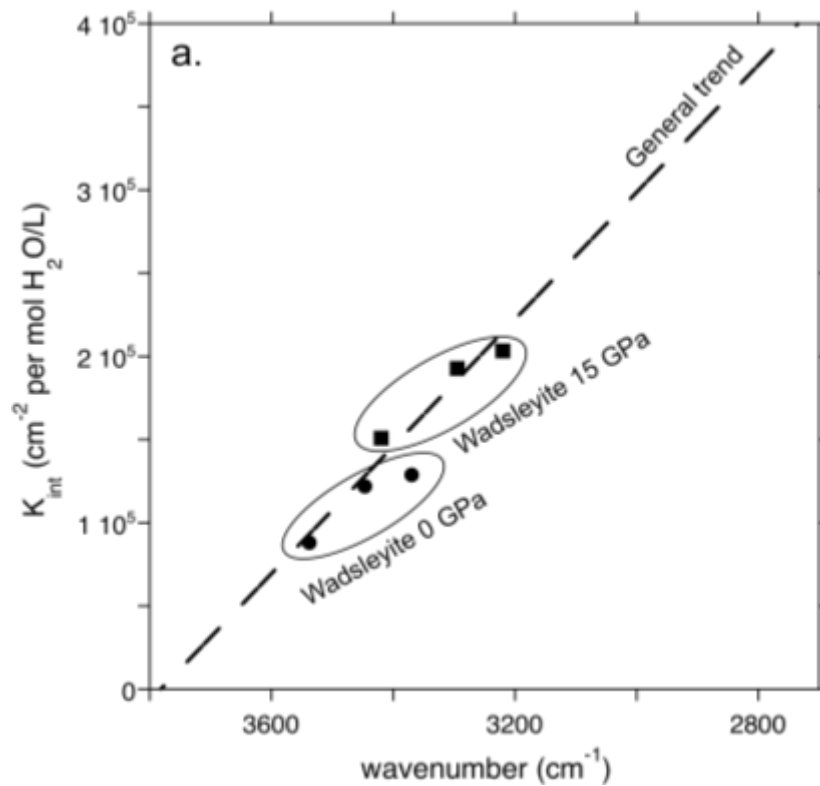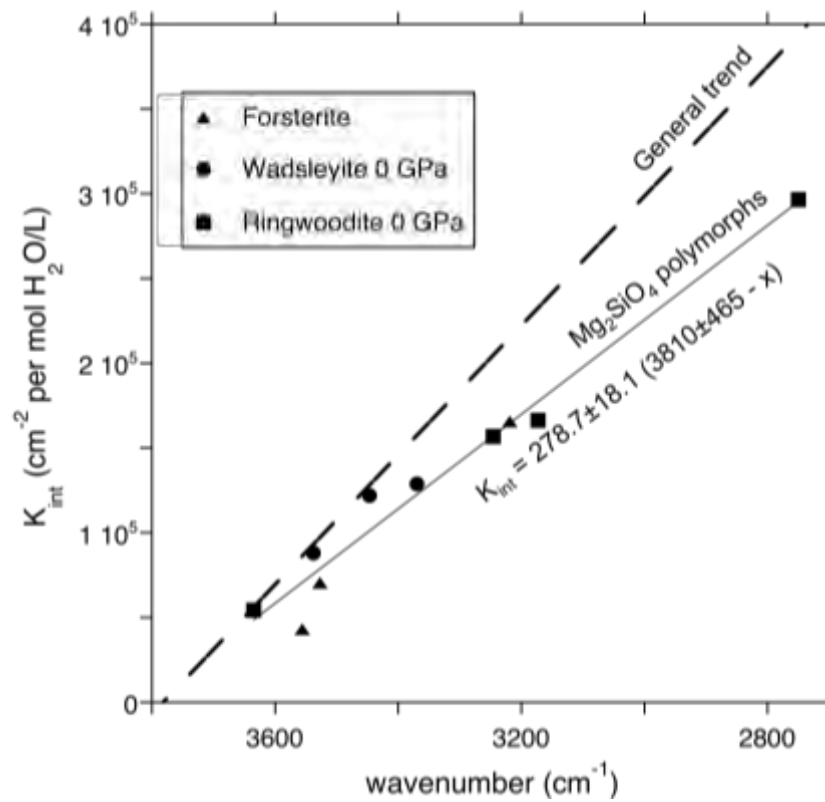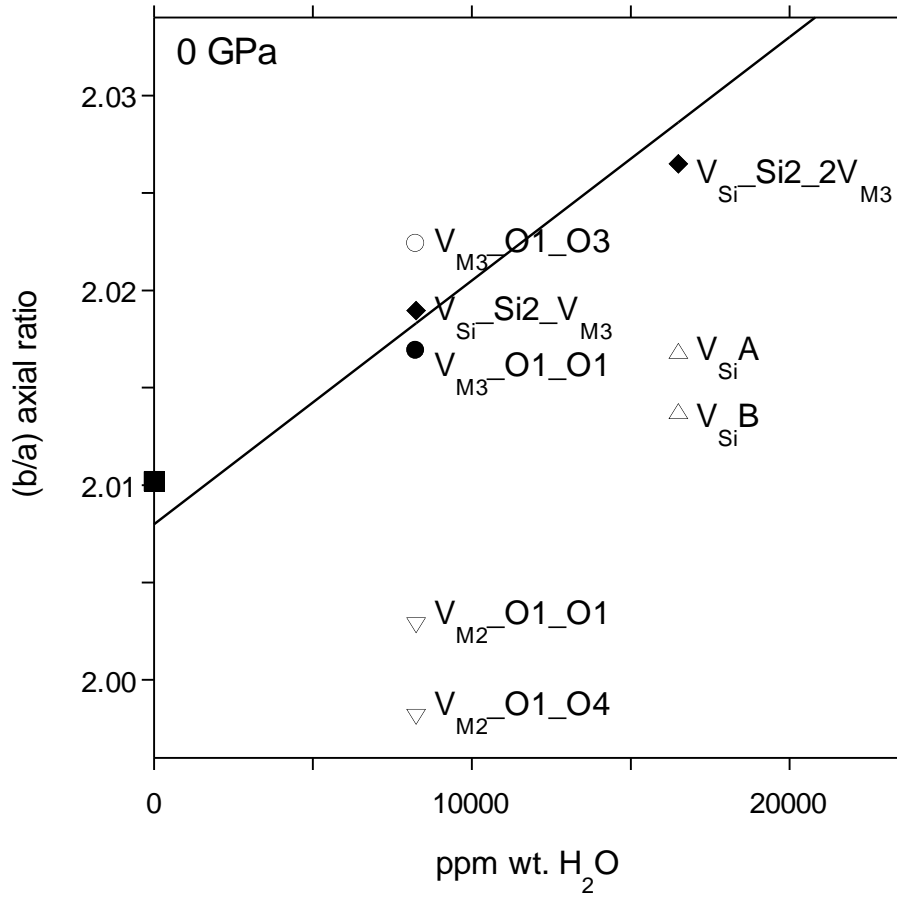682   Fig. 4

683

684

685   Fig. 5

686

38

687

688   Fig. 6

689

690

39

691

692

693   Fig. 7

694

695

696   Fig. 8